Editors' Suggestion | Featured in Physics

Phonon-Number-Sensitive Electromechanics

J. J. Viennot,* X. Ma, and K. W. Lehnert
JILA, National Institute of Standards and Technology and the University of Colorado, Boulder, Colorado 80309, USA
and Department of Physics, University of Colorado, Boulder, Colorado 80309, USA

(Received 8 August 2018; published 29 October 2018)

We use the strong intrinsic nonlinearity of a microwave superconducting qubit with a 4 GHz transition frequency to directly detect and control the energy of a micromechanical oscillator vibrating at 25 MHz. The qubit and the oscillator are coupled electrostatically at a rate of approximately $2\pi \times 22$ MHz. In this far off-resonant regime, the qubit frequency is shifted by 0.52 MHz per oscillator phonon, or about 14% of the 3.7 MHz qubit linewidth. The qubit behaves as a vibrational energy detector and from its line shape we extract the phonon number distribution of the oscillator. We manipulate this distribution by driving number state sensitive sideband transitions and creating profoundly nonthermal states. Finally, by driving the lower frequency sideband transition, we cool the oscillator and increase its ground state population up to 0.48 ± 0.13, close to a factor of 8 above its value at thermal equilibrium. These results demonstrate a new class of electromechanics experiments that are a promising strategy for quantum nondemolition measurements and nonclassical state preparation.

DOI: 10.1103/PhysRevLett.121.183601

The ability to bring manmade acoustical or mechanical structures into the quantum regime has been demonstrated in a variety of devices, from micromechanical oscillators in opto- and electromechanics experiments [1,2], to acoustic resonators in circuit quantum electrodynamics (cQED) experiments [3]. Mechanical oscillators are generally very linear harmonic oscillators at the quantum scale, and to achieve arbitrary quantum control, one needs an extrinsic nonlinearity [4]. Performing nonlinear detection is also a way to enable quantum nondemolition measurement by measuring energy instead of position or momentum [5–7]. One strategy is to use the Josephson junction used in superconducting microwave circuits. It provides a dissipationless strong nonlinearity and has enabled the demonstration of landmark results in quantum science from the preparation of arbitrary quantum states of microwave light [8,9] to the demonstration of early-stage quantum computers [10,11]. By using piezoelectric materials, resonant coupling between superconducting qubits and high frequency (GHz) acoustic wave resonators has been demonstrated [3,12].

This resonant approach is, however, restricted to a small class of acoustic oscillators and loses many of the advantages of the micromechanical oscillators used in opto- and electromechanics experiments [13]. In these experiments, a wide variety of techniques have been developed and have made these mass-on-a-spring-like oscillators very versatile. They can be used to interface otherwise incompatible quantum systems such as superconducting circuits and optical light [14], they are extraordinarily sensitive detectors of force and strain [15,16], and they can be engineered to have extremely long lifetimes [17]. However, these low frequency mechanical oscillators have proven to be more challenging to couple to superconducting qubits. One strategy is to use a linear cavity to transfer nonclassical microwave fields created by a qubit to a mechanical oscillator by using the radiation pressure interaction [18,19]. This approach has to battle the incompatibility of large microwave pump powers with qubits as well as the loss during the state propagation or transfer. Low frequency mechanical oscillators have also been directly coupled to qubits [20,21], but so far the interaction strengths have been too weak to achieve control or detection of motion at the scale of few phonons.

In this Letter, we directly couple a superconducting qubit to a mechanical oscillator, achieving an ultrastrong interaction of $g_m \approx 2\pi \times 22$ MHz, comparable to the oscillator's resonance frequency $\omega_m \approx 2\pi \times 25$ MHz. Similar to quadratic optomechanics proposals [6], we detect the energy of the oscillator instead of its position. More precisely, a mechanical ac-Stark effect shifts the qubit frequency by 0.52 MHz per oscillator phonon, or about 14% of the 3.7 MHz qubit linewidth. The qubit line shape therefore encodes the phonon number statistics, which we extract using a Bayesian-based algorithm. The qubit-oscillator system also exhibits blue and red sideband transitions, analogous to those found in optomechanics and trapped ions systems [13,22], at the sum (blue) and difference (red) of frequencies. In contrast to optomechanics, the qubit nonlinearity makes these sideband transitions number state dependent. Using this property, we demonstrate control of populations in the Fock space with a resolution of about 7 quanta. By driving the lower frequency sideband transition, we cool the oscillator and increase its ground state

population up to 0.48 ± 0.13, close to a factor of 8 above its value at thermal equilibrium.

Because our mechanical oscillator frequency is so low compared to that of a qubit at a few GHz, we require a qubit that couples statically to the oscillator. We achieve this interaction by forcing electrostatic charge onto the oscillator and using a Cooper-pair box qubit [23,24], which, unlike a transmon, is sensitive to charge at low frequency [25]. Our device is presented in Figs. 1(a) and 1(b), and it can be mapped on the circuit diagram of Fig. 1(c). The mechanical oscillator is an aluminum drumhead, similar to those used in previous electromechanics experiments [1]. It is suspended over two separate aluminum electrodes and realizes a mechanically compliant capacitor with each electrode. When the drum vibrates in its first harmonic, the regions of the drumhead located above the two bottom electrodes move with opposite phases, as depicted in Fig. 1(c). The two bottom electrodes are connected through two Josephson junctions in parallel, which hybridize the charge states of the two islands to form a flux tunable charge qubit [23,24]. We operate this qubit at the charge degeneracy point. The device is embedded in a far detuned coplanar waveguide resonator such that the qubit can be read out and coherently controlled using standard cQED techniques [26,27].

Our ability to apply a large dc bias on the drum is essential to the working principle of the device. When such a voltage is applied, a static charge accumulates on the capacitor's plates $C^{\pm}_{\mathrm{drum}}$ and this charge is forced to move along with the mechanical motion. The motion of this charge is equivalent to an ac voltage applied differentially over the qubit electrodes and creates a Josephson current going through the junctions at mechanical frequency. Mechanical motion is thus transversely coupled to the qubit transition, realizing a Rabi Hamiltonian with a coupling strength $g_m \approx 2\pi \times 3.7$ MHz/V. Most of the data we present were obtained with $V_d = 6$ V.

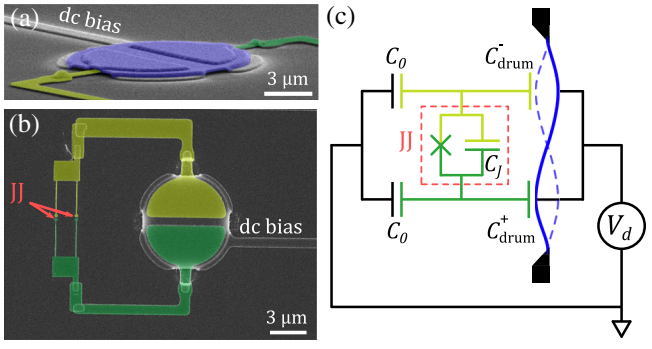

FIG. 1. (a) False-colored scanning electron micrograph (at an angle) of the micromechanical oscillator (blue) suspended above two electrodes and forming a vacuum gap capacitor. (b) Top view of the device showing the superconducting qubit electrodes (yellow and green), shunted by two Josephson junctions (JJ) in parallel. The dc bias line imposes a voltage V_d onto the oscillator plate. (c) Equivalent circuit of the device.

At zero bias voltage, the motion of the drum only modulates the capacitances of the qubit electrodes and the qubit-mechanics coupling is negligible. We can use this fact to characterize the bare qubit. Figure 2(a) shows a qubit spectroscopy at $V_d = 0$ V, obtained by measuring the qubit excited state probability P_e as a function of the frequency of a weak microwave drive. Fitting this to a Lorentzian, we obtain a FWHM of about $\Gamma^*_2 \approx 2\pi \times 3.7$ MHz, consistent with coherent control data in the time domain [27].

When a 6 V dc bias is applied on the drum, the qubit and the oscillator have a very large coupling strength ($g_m/\omega_m \approx 0.9$). Nevertheless, this device is in a regime where the mechanical frequency is more than 2 orders of magnitude smaller than the qubit frequency. In this limit, the two systems do not exchange energy spontaneously, but instead they shift each other's resonance frequency according to the effective Hamiltonian [26,41–43],

$$H/\hbar = \omega_m a^\dagger a + \frac{1}{2}(\omega_q + 2\chi_m a^\dagger a)\sigma_z, \qquad (1)$$

where a is the phonon annihilation operator, σ_z is the qubit Pauli operator, ω_q is the Lamb-shifted qubit frequency, and $\chi_m \approx 2g_m^2/\omega_q$ includes the Bloch-Siegert shift [43–45]. We determine $2\chi_m \approx 2\pi \times 0.52$ MHz by measuring how the mechanical oscillator frequency is dispersively shifted by

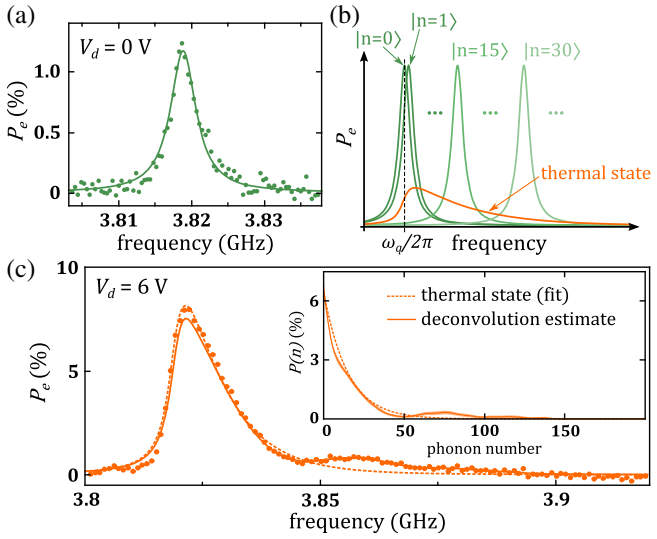

FIG. 2. (a) Low power spectroscopy of the qubit decoupled from the mechanical oscillator, at $V_d = 0$ V. The solid line is a Lorentzian fit indicating an intrinsic qubit linewidth of about 3.7 MHz. (b) Principle of the ac-Stark shift. The bare qubit resonance is shifted by a fraction of its linewidth for each number state. For a mechanical thermal state, the dressed qubit line shape is the sum over all number states weighted by their population. (c) Spectroscopy of the qubit coupled to the mechanical oscillator (at thermal equilibrium). Inset: Phonon populations extracted with a fit assuming a thermal distribution (dashed line) or with a Bayesian-based deconvolution algorithm (full line).

the qubit in its ground state [27]. Equation (1) shows how the qubit transition frequency is dressed by each phonon in the oscillator, $\tilde{\omega}_q(n) = \omega_q + 2\chi_m n$. This effect is sketched in Fig. 2(b). A figure of merit of our device is given by the ratio between the single phonon Stark shift and the qubit FWHM, $2\chi_m/\Gamma_2^* \approx 0.14$. In terms of resolution, this means that the sum of two phonon number states different by 7 or more will yield a qubit spectrum with two resolved peaks. As shown below, performing fits or deconvolutions allows us to go beyond this limit.

In order to determine the phonon number distribution from the ac-Stark shift, we make an approximation that treats the qubit line shape dressed by the mechanical motion as [46]

$$P_e^{\text{dressed}}(\omega) = \sum_n P(n) P_e^{\text{bare}}(\omega - 2\chi_m n), \qquad (2)$$

where $P_e^{\text{bare}}(\omega)$ is the response of the bare qubit to a spectroscopic drive at the frequency $\omega/2\pi$. The validity of this approximation depends on three conditions which are well satisfied for phonon numbers up ≈50 [27,47]. This keeps us from being quantitative for populations at larger phonon numbers with Eq. (2), but as discussed below, it allows us to make qualitative statements about arbitrary distributions.

The measured spectroscopy of the qubit dressed by the mechanical oscillator at thermal equilibrium with our dilution refrigerator is shown in Fig. 2(c). The asymmetry in the line shape reflects the thermal distribution of the oscillator, with a tail going to high Fock numbers. Assuming that the mechanical oscillator number state distribution is that of a thermal state, $P(n) = n_{\text{th}}^n/(n_{\text{th}}+1)^{n+1}$, we can fit this line shape using Eq. (2) with n_{th} as a fit parameter and we extract $n_{\text{th}} \approx 15$ (about 18 mK) [27]. This procedure only works for mechanical states for which we know the functional form of $P(n)$ (thermal states, coherent states, displaced thermal states, etc). In order to be more general, we use an adapted version of the Bayesian-based Lucy-Richardson algorithm to invert Eq. (2) [27,48]. The extracted $P(n)$ distribution is shown in Fig. 2(c), along with the distribution obtained assuming a thermal state. The reconstructed populations are plotted along with confidence intervals obtained from a nonparametric bootstrap [49]. The small bump in the data, just above 3.85 GHz, is a manifestation of a deviation from the small number of phonons approximation, which makes Eq. (2) inexact.

We now use the qubit to control the energy distribution of the mechanical oscillator by driving sideband transitions. Similar to opto- or electromechanics systems, we can drive a red or blue sideband transition. As depicted in Fig. 3(a), a red sideband transition excites the qubit while removing a phonon from the oscillator. Conversely, a blue sideband transition excites the qubit and adds a phonon to the oscillator. The crucial difference from that of conventional

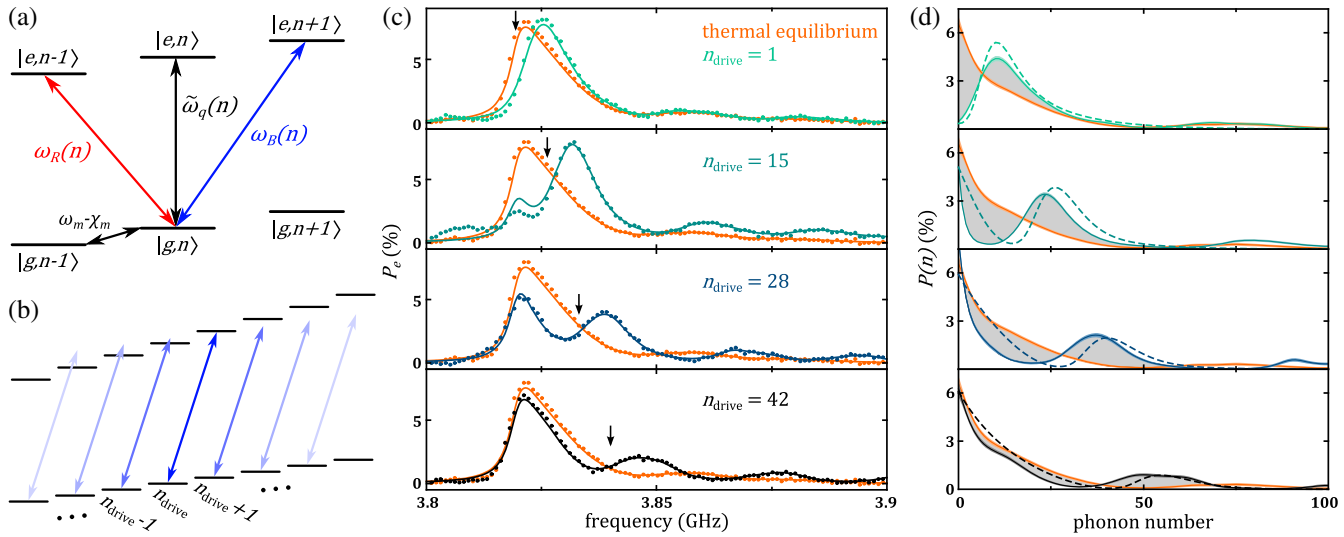

FIG. 3. (a) Energy level diagram for ground and excited states of the qubit (g and e), dressed by phonon numbers $n-1$, n, and $n+1$, showing the number-sensitive qubit transition $\tilde{\omega}_q(n)$ as well as the number-sensitive blue and red sideband transitions $\omega_{B(R)}(n)$. (b) For a blue sideband drive centered around n_{drive}, blue sideband transitions at neighboring number states are also driven, at a smaller rate. (c) Qubit spectroscopy after a blue sideband drive centered at a few different n_{drive}. Dots are raw data, full lines are qubit line shapes expected from the reconstructed phonon number distribution. Vertical black arrows indicate the position of n_{drive} mapped onto the spectroscopic frequency axis (that is, $\omega = \omega_q + 2\chi_m n_{\text{drive}}$). (d) Reconstructed experimental phonon populations (full lines) and master equation simulation (dashed lines) based on independently measured parameters. The orange curves, corresponding to the reconstructed populations of the thermal state, are shown for reference. Confidence intervals on the reconstruction (lighter shade) are obtained from a nonparametric bootstrap [27]. Gray areas show where populations have been moved by the sideband drive.

linear optomechanics is the number state dependence of these transitions. The blue (red) transition frequencies are given by

$$\omega_{B(R)}(n) = \omega_q \pm \omega_m + 2\chi_m\left(n \pm \frac{1}{2}\right). \tag{3}$$

Thus, driving a blue sideband transition at frequency $\omega_B(n_{\mathrm{drive}})$ only drives a few transitions at neighboring number states. The characteristic number of transitions being driven around n_{drive} is given by $\Gamma_2^*/2\chi_m$ [27], which is on the order of 7 transitions. Because these are two-photon transitions, we drive these sidebands with two tones: a lower frequency (260 MHz) dither applied to the Cooper-pair box gate, and a microwave tone detuned from the transition by the dither frequency [27], as proposed in Ref. [50].

Figure 3(c) shows qubit spectroscopies taken after a microwave pulse at a few different blue sideband frequencies, corresponding to transitions ranging from $n_{\mathrm{drive}} \approx 1$ to 42. When driving close to the ground state ($n_{\mathrm{drive}} \approx 1$), the dressed qubit resonance is essentially shifted to slightly higher frequency. However, driving at higher numbers qualitatively changes the qubit line shape, showing a first peak around the bare qubit frequency and a separate peak at higher frequency. This line shape reveals how the phonon populations are moved into distinct regions of the Fock space. The associated reconstructed phonon distributions $P(n)$ are given in Fig. 3(d). As highlighted by the shaded areas, these distribution show how our blue sideband pulse takes phonon populations around n_{drive} (or below) and transfers them to higher numbers. We can compare the reconstructed experimental phonon distributions with a semiclassical master equation simulation [dashed lines in Fig. 3(d)]. In these simulations, the qubit decoherence rates, the mechanical damping rate, the mechanical bath temperature, and the sideband rates are determined from independent measurements [27]. We attribute the difference between experiment and simulation mainly to deviations from Eq. (2) that yield inaccurate reconstructions. Nevertheless, the qualitative agreement between simulation and experimental data demonstrates how the qubit can be used to control the phonon population in the drum with a resolution of a few phonons and up to a relatively large number of phonons.

Finally, Fig. 4 shows how we use the qubit to cool thermal motion down with a red sideband drive. Cooling macroscopic mechanical motion with a superconducting qubit has been extensively investigated theoretically [51–55], but to our knowledge this is the first experimental demonstration of such a scheme. After a 150 μs red sideband pulse at $n_{\mathrm{drive}} \approx 8$, the population around $n = 8$ has been emptied and transferred to Fock numbers $n \leq 2$ (red data in Fig. 4). At this time, population at higher energy has not yet been affected because it is not in the

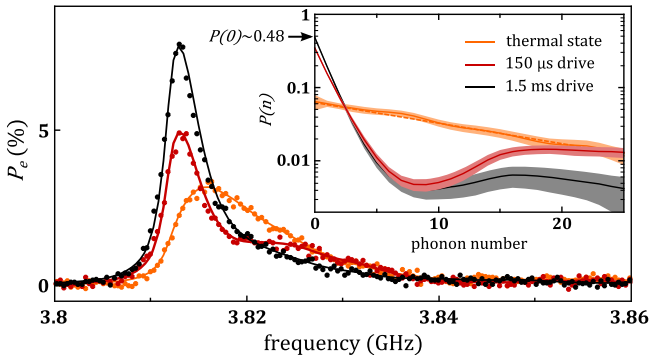

FIG. 4. Spectroscopy of the qubit after a red sideband drive of 150 μs (dark red) and 1.5 ms (black), centered around $n_{\mathrm{drive}} \approx 8$. Dots are raw data, full lines are qubit line shapes expected from the reconstructed phonon number distribution. Inset: Reconstructed experimental phonon populations (log scale, with bootstrap confidence intervals in lighter shades). The dotted line is the distribution of a fit to a thermal state. The horizontal black arrow indicates the ground state population of about 0.48 (see text).

number-sensitive window where the sideband drive is acting. Leaving the sideband drive on for a longer time, comparable to the mechanical damping time of about 1.7 ms, this higher number population slowly decays down into the range where the sideband drive is effective. This population is then also transferred to low phonon number and further increases the population around the mechanical ground state to reach $P(0) \approx 0.48 \pm 0.13$ (black data). The uncertainty on $P(0)$ is here dominated by our uncertainty in the bare qubit frequency [27] (uncertainty bands in Fig. 4 do not include this systematic effect). After this long pulse, the narrowed qubit line shape is a direct signature of the decreased phonon variance associated with lower mechanical temperature. For longer duration red sideband pulses, the drive begins to trivially heat the oscillator rather than cool it. Nevertheless, the demonstrated performance should be sufficient to prepare sub-Poissonian states at large average phonon number.

Looking forward, a natural next step would be to increase χ_m by increasing V_d. The maximum voltage we could apply in this study (6 V) was limited by our ability to read out the qubit through its dispersive coupling to the microwave resonator. For reasons we do not understand, the readout contrast diminished and became bistable with increasing voltage. Understanding and solving this problem would allow us to turn up V_d, in principle up to 21 V (limited by electrostatic instability). The single-phonon Stark shift $2\chi_m$ would then be approximately $2\pi \times 10$ MHz, exceeding the bare qubit linewidth and reaching the strong dispersive limit [56]. In addition, the ultrastrong qubit-mechanics interaction demonstrated here could also be combined with the microwave cavity to enter a rich three-body interaction regime [57]. This could be used to prepare nonclassical states such as mechanical cat

states and tripartite entangled states involving the microwave cavity, the qubit, and the mechanical oscillator.

We acknowledge Shlomi Kotler and Karl Mayer for enlightening discussions. We gratefully acknowledge Ray Simmonds and Florent Lecocq for their help with the fabrication of the device. We acknowledge fruitful discussions with Felix Beaudoin, Joe Aumentado, William Kindel, Michael Schroer, Lin Tian, Xian Wu, David Pappas, John Teufel, and Robert Lewis-Swan. We thank Maxime Malnou and Daniel Palken for providing us with a Josephson parametric amplifier. We acknowledge funding from National Science Foundation (NSF) under Grant No. 1125844 and from the Gordon and Betty Moore Foundation.

*viennot@jila.colorado.edu

[1] J. D. Teufel, T. Donner, D. Li, J. W. Harlow, M. S. Allman, K. Cicak, A. J. Sirois, J. D. Whittaker, K. W. Lehnert, and R. W. Simmonds, Nature (London) **475**, 359 (2011).
[2] J. Chan, T. P. M. Alegre, A. H. Safavi-Naeini, J. T. Hill, A. Krause, S. Gröblacher, M. Aspelmeyer, and O. Painter, Nature (London) **478**, 89 (2011).
[3] A. D. O'Connell, M. Hofheinz, M. Ansmann, R. C. Bialczak, M. Lenander, E. Lucero, M. Neeley, D. Sank, H. Wang, M. Weides, J. Wenner, J. M. Martinis, and A. N. Cleland, Nature (London) **464**, 697 (2010).
[4] S. L. Braunstein and P. van Loock, Rev. Mod. Phys. **77**, 513 (2005).
[5] C. M. Caves, K. S. Thorne, R. W. P. Drever, V. D. Sandberg, and M. Zimmermann, Rev. Mod. Phys. **52**, 341 (1980).
[6] J. D. Thompson, B. M. Zwickl, A. M. Jayich, F. Marquardt, S. M. Girvin, and J. G. E. Harris, Nature (London) **452**, 72 (2008).
[7] L. Dellantonio, O. Kyriienko, F. Marquardt, and A. S. Sørensen, Nat. Commun. **9**, 3621 (2018).
[8] M. Hofheinz, H. Wang, M. Ansmann, R. C. Bialczak, E. Lucero, M. Neeley, A. D. O'Connell, D. Sank, J. Wenner, J. M. Martinis, and A. N. Cleland, Nature (London) **459**, 546 (2009).
[9] B. Vlastakis, G. Kirchmair, Z. Leghtas, S. E. Nigg, L. Frunzio, S. M. Girvin, M. Mirrahimi, M. H. Devoret, and R. J. Schoelkopf, Science **342**, 607 (2013).
[10] J. Kelly *et al.*, Nature (London) **519**, 66 (2015).
[11] A. Kandala, A. Mezzacapo, K. Temme, M. Takita, M. Brink, J. M. Chow, and J. M. Gambetta, Nature (London) **549**, 242 (2017).
[12] Y. Chu, P. Kharel, W. H. Renninger, L. D. Burkhart, L. Frunzio, P. T. Rakich, and R. J. Schoelkopf, Science **358**, 199 (2017).
[13] M. Aspelmeyer, T. J. Kippenberg, and F. Marquardt, Rev. Mod. Phys. **86**, 1391 (2014).
[14] R. W. Andrews, R. W. Peterson, T. P. Purdy, K. Cicak, R. W. Simmonds, C. A. Regal, and K. W. Lehnert, Nat. Phys. **10**, 321 (2014).
[15] B. P. Abbott (LIGO Scientific Collaboration and Virgo Collaboration), Phys. Rev. Lett. **116**, 061102 (2016).
[16] J. Moser, J. Güttinger, A. Eichler, M. J. Esplandiu, D. E. Liu, M. I. Dykman, and A. Bachtold, Nat. Nanotechnol. **8**, 493 (2013).
[17] A. H. Ghadimi, S. A. Fedorov, N. J. Engelsen, M. J. Bereyhi, R. Schilling, D. J. Wilson, and T. J. Kippenberg, Science **360**, 764 (2018).
[18] F. Lecocq, J. D. Teufel, J. Aumentado, and R. W. Simmonds, Nat. Phys. **11**, 635 (2015).
[19] A. P. Reed, K. H. Mayer, J. D. Teufel, L. D. Burkhart, W. Pfaff, M. Reagor, L. Sletten, X. Ma, R. J. Schoelkopf, E. Knill, and K. W. Lehnert, Nat. Phys. **13**, 1163 (2017).
[20] M. D. LaHaye, J. Suh, P. M. Echternach, K. C. Schwab, and M. L. Roukes, Nature (London) **459**, 960 (2009).
[21] J.-M. Pirkkalainen, S. U. Cho, J. Li, G. S. Paraoanu, P. J. Hakonen, and M. A. Sillanpää, Nature (London) **494**, 211 (2013).
[22] D. Leibfried, R. Blatt, C. Monroe, and D. Wineland, Rev. Mod. Phys. **75**, 281 (2003).
[23] V. Bouchiat, D. Vion, P. Joyez, D. Esteve, and M. H. Devoret, Phys. Scr. **T76**, 165 (1998).
[24] Y. Makhlin, G. Schön, and A. Shnirman, Rev. Mod. Phys. **73**, 357 (2001).
[25] J. Koch, T. M. Yu, J. Gambetta, A. A. Houck, D. I. Schuster, J. Majer, A. Blais, M. H. Devoret, S. M. Girvin, and R. J. Schoelkopf, Phys. Rev. A **76**, 042319 (2007).
[26] A. Wallraff, D. I. Schuster, A. Blais, L. Frunzio, R.-S. Huang, J. Majer, S. Kumar, S. M. Girvin, and R. J. Schoelkopf, Nature (London) **431**, 162 (2004).
[27] See Supplemental Material at http://link.aps.org/supplemental/10.1103/PhysRevLett.121.183601 for additional details about device fabrication, measurement techniques, extended data, and modeling, which includes Refs. [28–40].
[28] J. D. Teufel, D. Li, M. S. Allman, K. Cicak, A. J. Sirois, J. D. Whittaker, and R. W. Simmonds, Nature (London) **471**, 204 (2011).
[29] G. J. Dolan, Appl. Phys. Lett. **31**, 337 (1977).
[30] A. Dunsworth *et al.*, Appl. Phys. Lett. **111**, 022601 (2017).
[31] A. Cottet, Implementation of a quantum bit in a superconducting circuit, Ph.D. thesis, Université Paris VI, 2002.
[32] J. Aumentado, M. W. Keller, J. M. Martinis, and M. H. Devoret, Phys. Rev. Lett. **92**, 066802 (2004).
[33] D. Gunnarsson, T. Duty, K. Bladh, and P. Delsing, Phys. Rev. B **70**, 224523 (2004).
[34] M. D. Shaw, R. M. Lutchyn, P. Delsing, and P. M. Echternach, Phys. Rev. B **78**, 024503 (2008).
[35] J. M. Martinis, M. Ansmann, and J. Aumentado, Phys. Rev. Lett. **103**, 097002 (2009).
[36] U. Vool, I. M. Pop, K. Sliwa, B. Abdo, C. Wang, T. Brecht, Y. Y. Gao, S. Shankar, M. Hatridge, G. Catelani, M. Mirrahimi, L. Frunzio, R. J. Schoelkopf, L. I. Glazman, and M. H. Devoret, Phys. Rev. Lett. **113**, 247001 (2014).
[37] R. W. Andrews, A. P. Reed, K. Cicak, J. D. Teufel, and K. W. Lehnert, Nat. Commun. **6**, 10021 (2015).
[38] L. B. Lucy, Astron. J. **79**, 745 (1974).
[39] D. Walls and G. Milburn, *Quantum Optics* (Springer, New York, 1994).
[40] A. J. Weinstein, C. U. Lei, E. E. Wollman, J. Suh, A. Metelmann, A. A. Clerk, and K. C. Schwab, Phys. Rev. X **4**, 041003 (2014).

[41] A. Blais, R.-S. Huang, A. Wallraff, S. M. Girvin, and R. J. Schoelkopf, Phys. Rev. A **69**, 062320 (2004).
[42] D. I. Schuster, A. Wallraff, A. Blais, L. Frunzio, R.-S. Huang, J. Majer, S. M. Girvin, and R. J. Schoelkopf, Phys. Rev. Lett. **94**, 123602 (2005).
[43] F. Beaudoin, J. M. Gambetta, and A. Blais, Phys. Rev. A **84**, 043832 (2011).
[44] F. Bloch and A. Siegert, Phys. Rev. **57**, 522 (1940).
[45] D. Zueco, G. M. Reuther, S. Kohler, and P. Hänggi, Phys. Rev. A **80**, 033846 (2009).
[46] J. Gambetta, A. Blais, D. I. Schuster, A. Wallraff, L. Frunzio, J. Majer, M. H. Devoret, S. M. Girvin, and R. J. Schoelkopf, Phys. Rev. A **74**, 042318 (2006).
[47] A. A. Clerk and D. W. Utami, Phys. Rev. A **75**, 042302 (2007).
[48] W. H. Richardson, J. Opt. Soc. Am. **62**, 55 (1972).
[49] B. Efron and R. Tibshirani, *An Introduction to the Bootstrap* (Chapman and Hall, London, 1994), p. 436.
[50] A. Blais, J. Gambetta, A. Wallraff, D. I. Schuster, S. M. Girvin, M. H. Devoret, and R. J. Schoelkopf, Phys. Rev. A **75**, 032329 (2007).
[51] I. Martin, A. Shnirman, L. Tian, and P. Zoller, Phys. Rev. B **69**, 125339 (2004).
[52] P. Zhang, Y. D. Wang, and C. P. Sun, Phys. Rev. Lett. **95**, 097204 (2005).
[53] J. Hauss, A. Fedorov, C. Hutter, A. Shnirman, and G. Schön, Phys. Rev. Lett. **100**, 037003 (2008).
[54] K. Jaehne, K. Hammerer, and M. Wallquist, New J. Phys. **10**, 095019 (2008).
[55] P. Rabl, Phys. Rev. B **82**, 165320 (2010).
[56] D. I. Schuster, A. A. Houck, J. A. Schreier, A. Wallraff, J. M. Gambetta, A. Blais, L. Frunzio, J. Majer, B. Johnson, M. H. Devoret, S. M. Girvin, and R. J. Schoelkopf, Nature (London) **445**, 515 (2007).
[57] M. Abdi, M. Pernpeintner, R. Gross, H. Huebl, and M. J. Hartmann, Phys. Rev. Lett. **114**, 173602 (2015).